Risk Assessment of Rehabilitation Strategies for Steel Lattice Telecommunication Towers of Greece under Extreme Wind Hazard

Authors: Dimitrios V. Bilionis[1], Konstantinos Vlachakis[2], Dimitrios Vamvatsikos[3] Maria-Eleni Dasiou[2], Ioannis Vayas[4], Konstantinos Lagouvardos[5]

Abstract

The risk and losses associated with the wind-induced failure of existing steel lattice telecommunication towers are assessed for a number of upgrade/replace/redesign schemes. Specifically, a performance-based wind engineering framework is employed for assessing a typical tower topology used by EU telecommunication network operators over four different cases: a conventional design, its corroded version after 60 years, a strengthened version of the corroded tower by applying fibre-reinforced polymer plates, and a redesign with high-strength steel. Multiple potential sites of installation were considered throughout coastal and mainland Greece, comprising two different groups of design wind speed. Mischaracterization of the site-specific wind distribution is by far the most important risk factor, with corrosion coming right behind. Still, selecting a rehabilitation approach does not depend only on site and tower characteristics, but also on the projected direct and indirect losses. By considering service to different populations, even after 60 years of corrosion, the "Do Nothing" approach may still be competitive when serving few residents and for short projected lifetime, while an upgrade is considered optimal for larger towns, or wherever higher revenue is on the line.

Keywords: telecommunication tower; steel lattice tower; performance-based wind engineering; risk assessment; wind hazard

1. INTRODUCTION

Telecommunication towers constitute critical components of infrastructure in modern societies. Rapid advances in data transmission technology introduce new engineering challenges affecting both the electromechanical equipment and the supporting structures of telecommunication networks. Supporting structures are usually tall highly-optimized steel lattice towers with wind actions being the governing loading condition, rather than the dead-loads of the steel members and the microwave antennas.

The design and analysis of telecommunication towers have attracted considerable research interest. For example, tower failure mechanisms under wind loading have been

[1] PhD Candidate, Institute of Steel Structures, School of Civil Engineering, National Technical University of Athens, Greece (corresponding author). E-mail: dimbilionis@central.ntua.gr

[2] PhD Candidate, Institute of Steel Structures, School of Civil Engineering, National Technical University of Athens, Greece. E-mail: kostasvlachakis@central.ntua.gr (K. Vlachakis), medasiou@mail.ntua.gr (M.-E. Dasiou)

[3] Associate Professor, Institute of Steel Structures, School of Civil Engineering, National Technical University of Athens, Greece. E-mail: divamva@mail.ntua.gr

[4] Professor, Institute of Steel Structures, School of Civil Engineering, National Technical University of Athens, Greece. E-mail: vastahl@central.ntua.gr

[5] Research Director, Institute for Environmental Research and Sustainable Development, National Observatory of Athens, Athens, Greece. E-mail: lagouvar@noa.gr

investigated in [1]-[4], while topology optimization has been tackled by [5]. Moreover, network upgrades are usually associated with the addition of new equipment (e.g. microwave antennas) on existing towers leading to additional strength and stability verifications [6] and also in strengthening interventions [7]. The effect of adverse wind conditions is further enhanced when ice has accumulated on the exposed members due to low temperature and/or precipitation causing tower failures especially in cold regions [8]-[10].

Considering the above, the risk assessment of telecommunication towers mainly under wind actions is of high interest. Risk assessment can be performed under a Performance Based Engineering (PBE) framework, first introduced in Earthquake Engineering [11]. Since then, the application of PBE has been expanded rapidly to other fields of structural engineering, including wind [12]-[13]. Performance Based Wind Engineering (PBWE) has been applied to numerous structures affected by winds such as: tall buildings [14]-[17]; long span suspension bridges [12]; offshore wind turbines [18]; and recently in telecommunication towers [19]-[20].

Herein, a PBWE framework is applied for assessing the risk of a telecommunication tower topology designed according to EN standards for use in Greece. Four different cases are considered, comprising a conventional design, a corroded, a strengthened and a high-strength steel version. For all cases the risk is estimated by evaluating the weather hazard of multiple installation sites throughout Greece, as revealed by the analysis of all available meteorological data. Finally, an illustrative cost-benefit analysis example is presented pointing out the application of the proposed framework as a decision tool for stakeholders.

2. PERFORMANCE-BASED ENGINEERING FRAMEWORK

According to the Pacific Earthquake Engineering Research (PEER) Center [11] the structural risk can be defined in terms of the mean annual frequency (MAF), $\lambda(DV)$, of a given decision variable, *DV*:

$$\lambda(DV) = \iiint G(DV|DM) \cdot |\mathrm{d}G(DM|EDP)| \cdot |\mathrm{d}G(EDP|IM)| \cdot |\mathrm{d}\lambda(IM)| \qquad (1)$$

As a *DV* can be considered any variable, such as cost, time (e.g. down-time of service) or casualties, that could be utilized by stakeholders in decision making. *DM* represents the damage measure and is usually discretized in a definite number of damage states (e.g. operational, life safe, structural safe, collapse). *DM* should be defined based on one or more Engineering Demand Parameters (*EDP*) such as: roof drift, roof displacement, etc. Finally, *IM* stands for a scalar or vector intensity measure (e.g. wind speed, or wind speed and direction) and is associated with the natural hazard. In Eq. (1) the notation $\lambda(\cdot)$ corresponds to the MAF of its argument, while $G(x|y)$ is the conditional complementary distribution function of x given y.

Following [21], Eq. (1) can be simplified to the following form:

$$\lambda(DV) = \int G(DV|IM) \cdot |\mathrm{d}\lambda(IM)| \qquad (2)$$

The *DV* could be a limit state of the structure, i.e., an event associated with the violation of a specific threshold of interest. Typically, this is expressed in terms of the demand, *D*, exceeding capacity, *C*, transforming Eq. (2) to become:

$$\lambda(D > C) = \int P(D > C|IM) \cdot |\mathrm{d}\lambda(IM)| \quad (3)$$

where $P(D > C|IM)$ is the probability of $D > C$ given the *IM*, or the fragility of the structure, while $\mathrm{d}\lambda(IM)$ is the hazard differential. Natural hazards are site-specific and independent of the structure. On the other hand, fragility depends only on the structure's characteristics (such as: condition, strength, etc.). Overall, following Eq. (3), the risk of a structure is a convolution of the structure's fragility with the hazard of the installation site.

3. TELECOMMUNICATION TOWER CASE STUDIES

3.1. Geometry

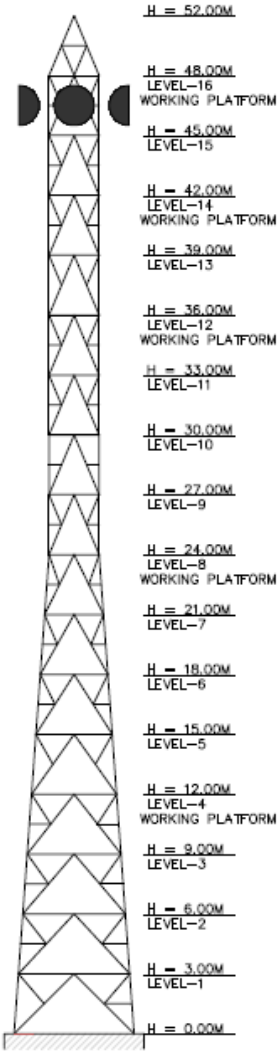

a)

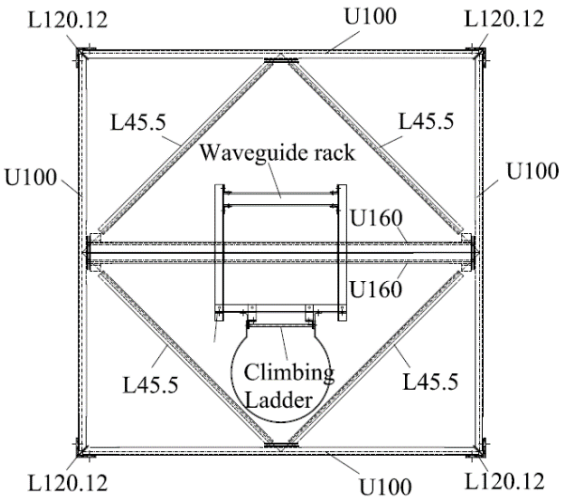

b)

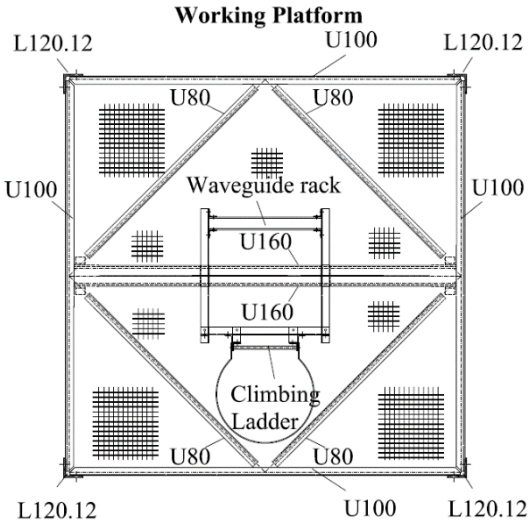

c)

Figure 1: a) Tower elevation; b) typical plan of a horizontal diaphragm; c) typical plan of a working platform [22].

The main body of the lattice tower studied is 48 meters tall and has a square cross section [22]. At the top of the tower, a pyramid that holds the lightning rod is placed and ends at a height of 51 m. A complete view of the tower is presented in Figure 1a. The view of the tower can be divided into two main sections: an inclined section, whose square cross section decreases with height and runs from 0 to 24 m and a straight section, which runs from 24 to 48 m and has no inclination with respect to the vertical, since it is designed to carry the antennas. The tower has horizontal diaphragms every 3 meters along its height (Figure 1b). It also includes five working platforms at heights of 12, 24, 36, 42 and 48 m (Figure 1c). Finally, a ladder and a waveguide rack for the cables of the antennas run through the centers of the horizontal diaphragms.

The structural members of the tower consist of angle and channel steel sections. The members can be characterized per Figure 2 as: legs, (main) vertical diagonals/bracing members, secondary vertical bracing members, horizontals, horizontal diagonals, and a central horizontal member at each diaphragm which carries the loads of the ladder, the waveguide rack and the signal-transferring cables. All legs are pinned at the foundation.

The four tower versions were modeled in OpenSees [23]. Each of the final 3D models was composed of 932 members, utilizing both fiber-section force-based beam-column elements (legs and main diagonals) and truss elements (others). The buckling of single angle members is a complex phenomenon (see [24]-[25]). To capture the effect of member buckling, a hysteretic material curve was employed, following the general shape of Figure 3. This shape is adjusted according to the characteristics of each member to capture its tension, compression and bending behavior. Specifically, the buckling reduction factor χ was calculated for each structural member according to EN 1993-3-1 [26] to reduce its compression strength, while a uniform value of Young's Modulus, $E = 210$ GPa, was applied. In general, the post-buckling and hysteretic behavior would be of interest to determine the global performance after the first occurrence of buckling; yet, the optimized shape of the lattice tower means that this event is quickly followed by global collapse (see Section 3.4). Thus, little attention needs to be paid to these details of the material behavior.

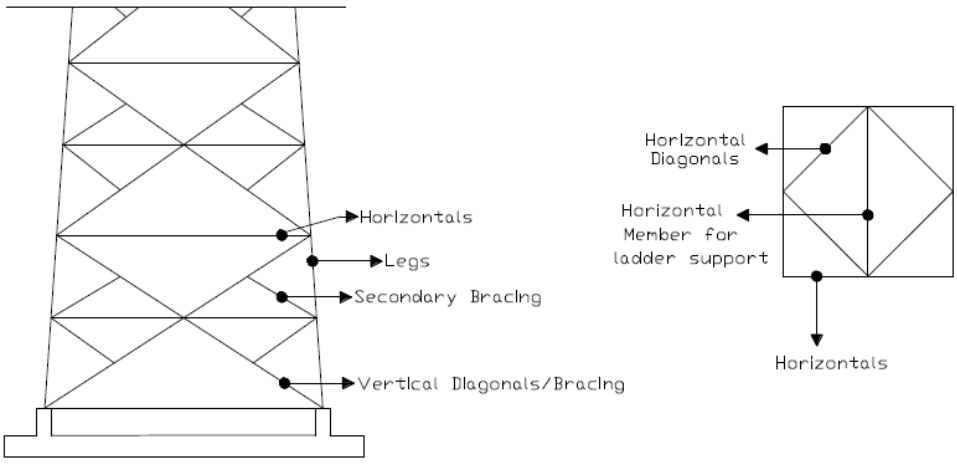

Figure 2: Designation of structural members [22].

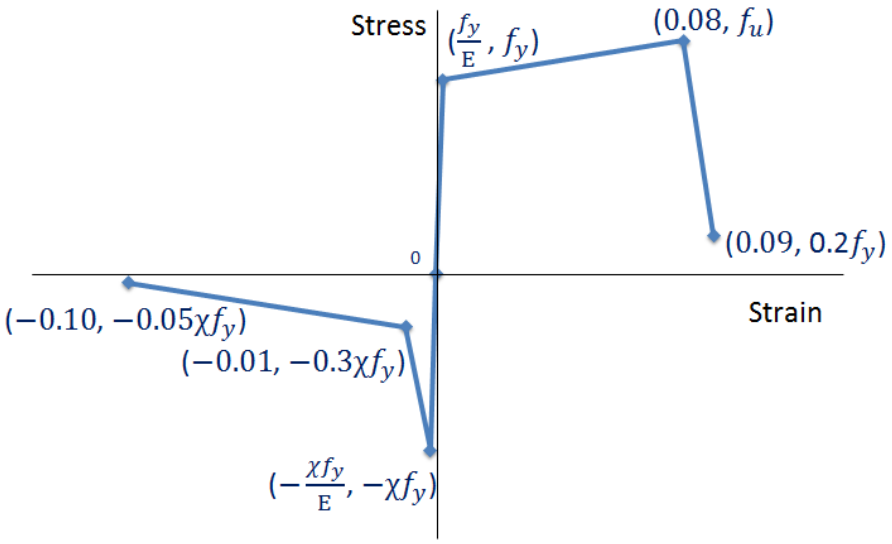

Figure 3: General form of a member (material) stress-strain curve

3.2. Loads

Gravity loads

The weight of the climbing ladder is 15.30 kN and the weight of waveguide rack 14.60 kN. Four dish antennas are installed at the top (height 45–48 m) of the tower. Each dish antenna has a weight of 2.30 kN. The weight of the cables is assumed to be 0.05 kN/m per dish. Finally, the weight of the five working platforms is 0.25 kN/m^2. The live load of the climbing ladder is 5.00 kN, while the live load at the working platforms is assumed to be 2.00 kN/m^2.

Wind loads

In the case of a telecommunication tower with dish antennas, the total wind force acting on the structure consists of two main components, namely the force acting on the tower (i.e. the structural members) and the force acting on the dish antennas [27]-[29].

Wind load on tower body

The wind force acting on each discrete level at height z of the tower is calculated as:

$$F_{body}(z) = qC_DA_{ref} \quad (4)$$

where q is the dynamic pressure of the wind, C_D is the drag coefficient and A_{ref} is the area of the members, pertinent to said tower level, projected normal to the level of the wind. The dynamic pressure of the wind q depends on the air density ρ = 1.225 kg/m^3, and the wind speed u:

$$q = \frac{1}{2}\rho u^2 \quad (5)$$

The drag coefficient C_D for lattice steel structures depends on the solidity ratio φ. According to EN1991-1-4 [30], φ is the fraction of the sum of the projected area A of the members of the structure's face normal to that face divided by the total enclosed area A_c by the face's boundaries projected normal to the face:

$$\varphi = \frac{A}{A_c} \tag{6}$$

To determine φ and C_D, the tower was divided into sixteen segments every 3m along its height considering each horizontal diaphragm to be at the middle of the segment. The wind loads of each segment were assigned to the level of the corresponding diaphragm, accounting for the wind speed at each elevation using a power law profile (see Eq. (8)).

Wind load on dish antennas

According to [29], the commonly used practice for the estimation of the wind forces on dish antennas was to calculate the drag coefficient of each isolated antenna. However, this practice would overestimate the total force since the antenna may shield part of the tower. This is also evident when multiple antennas are installed at the same height. For this reason, except for the drag coefficient of the isolated antenna, an additional interference factor should be added. Thus, the wind force in case of two identical in size antennas installed at the same height is calculated as follows [27]-[28]:

$$F_{\text{antennas}} = qA_a(C_{Da_1}f_{a_1} + C_{Da_2}f_{a_2}) \tag{7}$$

where q is the dynamic pressure of the wind per Eq. (5), A_α is the area of each antenna projected normal to the level of the wind, $C_{D\alpha 1}$ and $C_{D\alpha 2}$ are the drag coefficients for the two isolated antennas and $f_{\alpha 1}$ and $f_{\alpha 2}$ are the corresponding interference factors for each of the antennas. The values of the drag coefficients and the interference factors of the antennas are mainly based on the wind angle and the solidity ratio. Those values are usually estimated experimentally [27]-[28]. Herein, proposed values by an experimental study of a similar case [28] were adopted.

Wind field simulation

To account for the dynamic variation of wind speed and associated loads along the height, multiple 2D wind fields were simulated via TurbSim [31]. These comprise spatially correlated 10-min wind speed timehistories over a planar 2D grid of points given a (reference) mean wind speed. At each point, all three wind speed components (for each of the three directions X, Y, Z) are simulated, with only the two horizontals being of interest for the tower assessment, since the vertical component is of negligible magnitude. To capture the variation of wind along the height, a power law wind speed profile was considered:

$$\frac{u(z)}{u_{ref}} = \left(\frac{z}{z_{ref}}\right)^a \tag{8}$$

where $u(z)$ is the wind speed at height z, u_{ref} is the wind speed at a reference height z_{ref}, and α is the power law exponent. A power law exponent $\alpha = 0.20$ was used, as proposed by IEC 61400-1 [32] for onshore structures. Herein, the values of wind speed at the heights of the horizontal diaphragms and the center of the dish antennas were calculated, resulting to wind loads along the height of the tower per Eq. (4) and Eq. (7). The wind speed $u(z)$ and the total wind load $F_T(z)$ profiles are presented in Figure 4. Both profiles follow similar patterns with the only difference observed at the height of the dish antennas due to the additional force added by the latter.

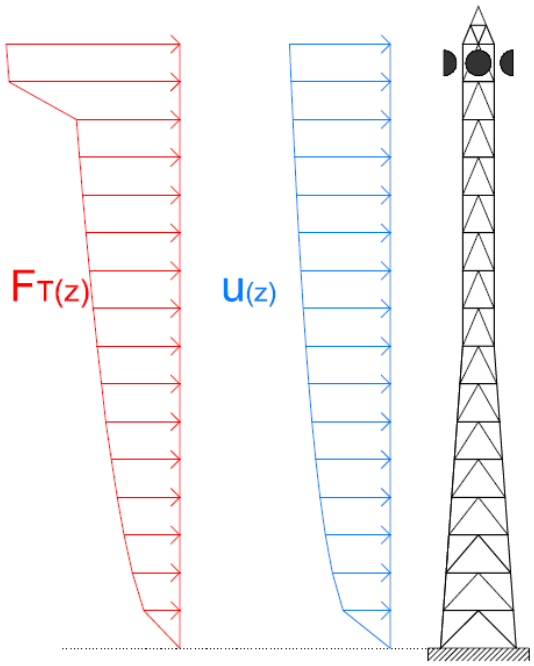

Figure 4: Profiles of wind speed $u(z)$ and total (body + antennas) wind force $F_T(z)$.

3.3. Tower Case Studies

Four different versions of the telecommunication tower were analyzed: a) an initial design according to EN standards using conventional steel; b) a corroded version of (a) at the end of an expected service life of 60 years; c) a strengthened version of (b) with selective application of fibre-reinforced polymer (FRP) plates, and d) a redesigned tower with high-strength steel (HSS) members. The latter two cases were selected in order to explore possible rehabilitation strategies of the corroded tower as it will be presented in Section 7. It is also noteworthy that strengthening via FRP plates is a relatively novel, easily applied and low-cost technique. On the other hand, the use of HSS can provide similar or even higher strength of the structure with lower weight (i.e. amount of steel).

In the initial design (initial tower), two types of angle sections were used for the legs. Specifically, in dimensions of mm the legs of the inclined section (height: 0-24 m) were L160.160.15, while the legs of the vertical section (height: 24-48 m) were L120.120.12. For the vertical bracing diagonals, L70.70.7 was used throughout the whole height of the structure, while for the secondary bracing L45.45.5 was employed. The horizontal members of each diaphragm were channel U100 sections. For the horizontal diagonal members angles L45.45.5 were used, except for the five levels of the working platforms where a channel U80 section was employed. The central horizontal member (for ladder support) of each diaphragm was formed by a built-up section composed of 2 closely-spaced channel U160 sections. Finally, the cross sections of the pyramid at the top of the tower (height: 48-51 m) were L70.70.7. The structural steel grade was S235 [33] for all tower members. For the performance assessment mean values of f_y = 328.80 MPa and f_u = 435.41 MPa were adopted as the yield and ultimate stress, respectively [34], in order to build the stress-strain curve of each element per Figure 3.

For the corroded tower, an atmospheric environment of category C4 was assumed, corresponding to high corrosivity, consistent with industrial areas or with coastal areas of moderate salinity [35]. Furthermore, the thickness of zinc layer (galvanization) at the beginning of service was considered equal to 40 μm. According to ISO 9224 [36], a zinc corrosion rate of 4 μm/yr was considered. Thus, the zinc layer was eliminated during the first 10 years of service. This value is considered for illustration purposes and may not necessarily represent standard practice, as corrosion protection is typically designed for a longer lifetime. For the bare carbon steel section under category C4, the corrosion rate was assumed to be 20 μm/yr during the first 10 years after zinc exhaustion and 15 μm/yr thereafter. The resulting loss of section thickness is presented in Figure 5. After 60 years of service life, all the members of the tower uniformly lost 0.8 mm of steel per exposed surface (neglecting localized higher losses due to pitting corrosion) for a total of 1.6 mm reduction of angle/channel section thickness.

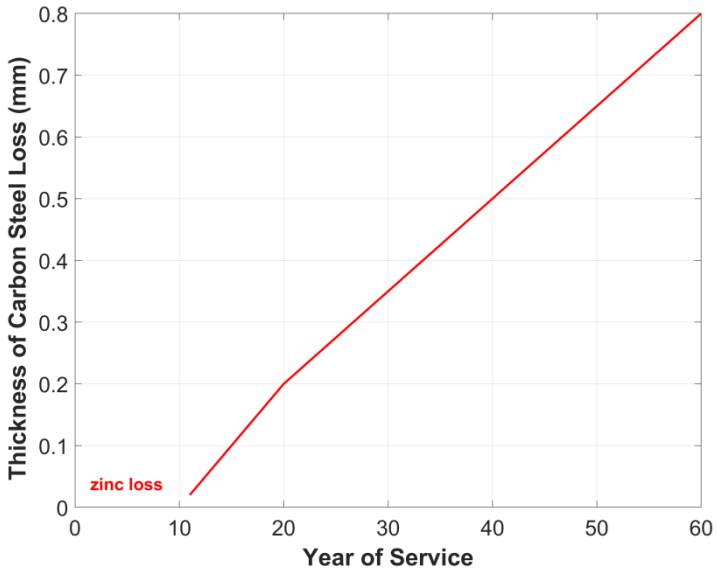

Figure 5: Uniform loss of thickness per exposed surface during service life of the telecommunication tower.

The third version of the telecommunication tower considered was the result of strengthening the corroded tower by the selective application of FRP plates. FRP plates can be attached on a corroded steel member (after sanding down any rust and paint products) resulting to a strengthened hybrid member with increased buckling and tension resistance [37]-[38]. Thanks to the minimal thickness and weight of the FRP, the overall weight and the corresponding wind reference area remain the same with the original (of corroded tower) steel members, rendering this strengthening approach a competitive alternative for steel lattice towers.

For the case at hand, preliminary pushover analyses utilizing a load pattern proportional to the total wind force (See Figure 4 and Section 3.4) indicated the L70.7.7 vertical diagonal members at heights of 24–33 m (where the leg inclination changes) to be the most vulnerable part of the tower (Figure 6). Twin 50mm x 1.2mm FRP plates were applied externally, one per each angle leg (Figure 7), with mean properties of E = 170 GPa and f_u = 3100 MPa. The tension and the buckling resistance of the new hybrid members were assessed as per [39]. Since the failure modes of the tower remain the same, whereby first member buckling swiftly leads to global collapse, the details of FRP material behavior do not matter beyond the increased hybrid member strength.

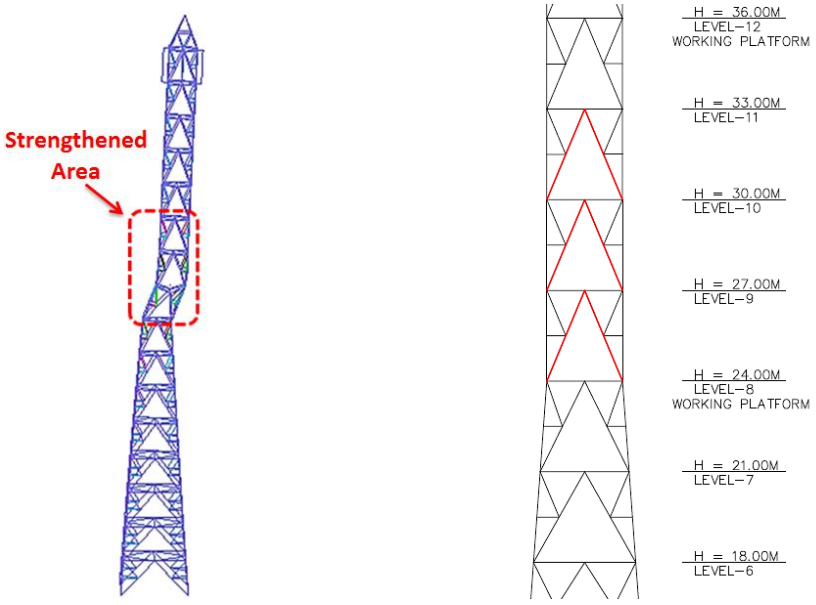

Figure 6: a) Failure pattern of tower where the red rectangle indicates the three levels to be strengthened; and b) detailed view of the diagonals strengthened via FRP (in red)

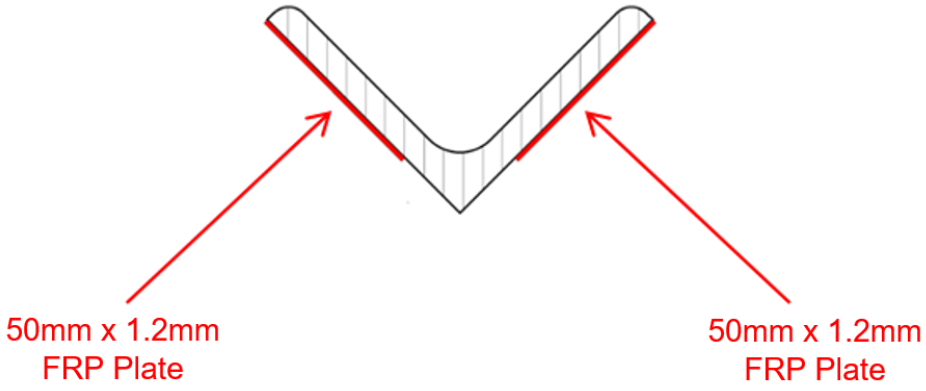

Figure 7: Hybrid member composed of existing angle section and FRP plates attached externally

The redesigned HSS version employed the geometry of the initial design, with steel grade S460 for the legs and the main bracing diagonal members, and S355 for all others. Mean values for the yield and ultimate stresses were taken from [34]: f_y = 495.26 MPa, f_u = 620.98 MPa for S460, and f_y = 414.09 MPa, f_u = 546.16 MPa for S355. As expected, smaller member sections ensued (see Table 1), leading to reduced self-weight, global stiffness, and wind reference area. Overall, the use of HSS reduces the total mass of the specific tower topology by 7.3%, or about 1,110 kg.

Table 1: Member sections in Initial versus HSS Tower

Member Type	Initial Tower		HSS Tower	
	Section	Steel Grade per [33]	Section	Steel Grade per [33]
Leg (inclined part)	L160.160.15	S235	L140.140.15	S460
Leg (vertical part)	L120.120.12	S235	L110.110.12	S460
Vertical Diagonal/Main Bracing Diagonal	L70.70.7	S235	L60.60.6*	S460
Secondary Bracing	L45.45.5	S235	L45.45.5	S355
Horizontal Diagonal	U80**	S235	U80**	S355
Horizontal	U100	S235	U100	S355
Horizontal Member for ladder support	2U160	S235	2U160	S355
Total mass of steel members (kg)	15140		14030	

* L70.70.7 was used for Vertical Diagonals at heights of 24 – 33 m.

** U80 was used for Horizontal Diagonals at the working platforms and L45.45.5 elsewhere.

Table 2 shows the first three natural periods for each of the four versions of tower. The first two modes have the same period due to structure's and loads symmetry, although they refer to different directions (X and Y). The third mode is torsional (Figure 8). As evident, the reduction of steel sections due to corrosion increased all three periods by about 8%. Subsequent strengthening by FRP did not make any appreciable difference as it adds negligible mass, only improving the strength of some sections with minor changes in their stiffness. Finally, for the HSS tower, the reduction in steel mass and global stiffness relative to the initial one ended up with a slightly increased period by 7%.

Table 2: First Three Natural Periods for each of the four versions of tower

Tower Version	T_1 (sec)	T_2 (sec)	T_3 (sec)
Initial Tower	0.83	0.83	0.28
Corroded Tower	0.90	0.90	0.32
Strengthened Hybrid Member Tower	0.90	0.90	0.32
HSS Tower	0.89	0.89	0.30

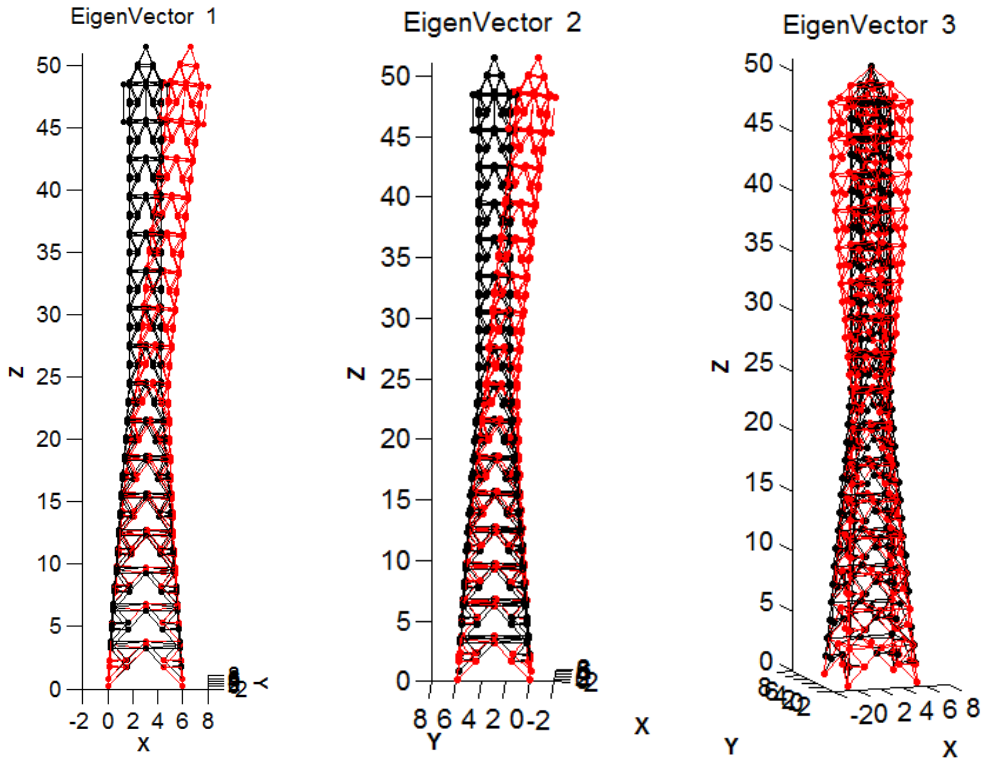

Figure 8: First three modes of tower

3.4. Analysis Results

In all cases, pushover (nonlinear static) analyses were performed. The lateral load profile considered follows the pattern of the wind force as shown in Figure 4. Given that dynamic analysis will impose a variable load pattern, while member capacities are also non-deterministic, a sensitivity analysis was also performed. Specifically, multiple pushover analyses were performed on each tower, employing small changes (up to 15%) on the material stress-strain relationship per Figure 3. Depending on the details of the material behavior employed for each member, the first failure is either from leg buckling (Figure 9a) or from main vertical bracing member buckling (Figure 9b), with the latter being prevalent for the case at hand. In both cases, the failure occurs at the height where the inclined legs become vertical, with an accompanying cross-section reduction. As lateral loads increase, the failure quickly cascades to other elements resulting to global collapse. Note that in all cases, fatigue does not govern failure, a finding also supported by empirical data on such tower typologies. Therefore, fatigue is completely disregarded, and the pushover results can be taken to offer a comprehensive view of the tower failure modes.

Figure 10 presents the pushover curves for each of the four towers. The horizontal axis depicts the displacement at the top along the lateral load direction, while the vertical axis depicts the Load Factor (*LF*), defined as the ratio of the total lateral load (or the total wind load) applied divided by its corresponding value at the basic design wind speed of 33 m/s calculated as per [30]. According to Figure 10 the HSS tower has the highest strength, since its failure occurs at *LF*=2.00. Note that this observation is not generalizable, as this higher system strength is not imparted by the material properties. After all, the same design standards are employed as in the case of the conventional steel initial design. Rather this is a consequence of the constraints of the catalogue of HSS angle sections offered by producers, which does not always allow a full

optimization of all members. On the other hand, as expected, the lowest value of *LF*=1.20 corresponds to the corroded tower. The initial tower lies somewhere in the middle with *LF*=1.57. Moreover, this value is almost equal to that of the strengthened tower at *LF*=1.59, showing that the FRP strengthening has fully restored the initial strength, despite the corrosion.

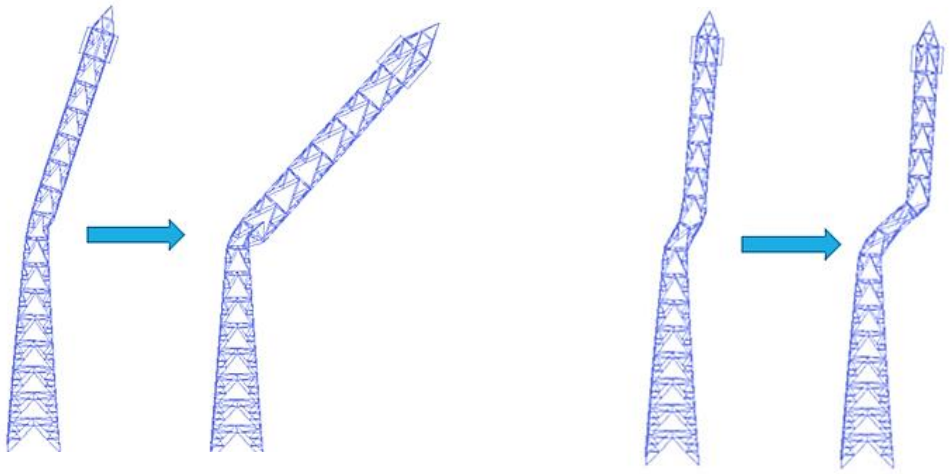

a) b)

Figure 9: Failure modes revealed by pushover analysis: a) Leg buckles first, b) Vertical bracing member buckles first.

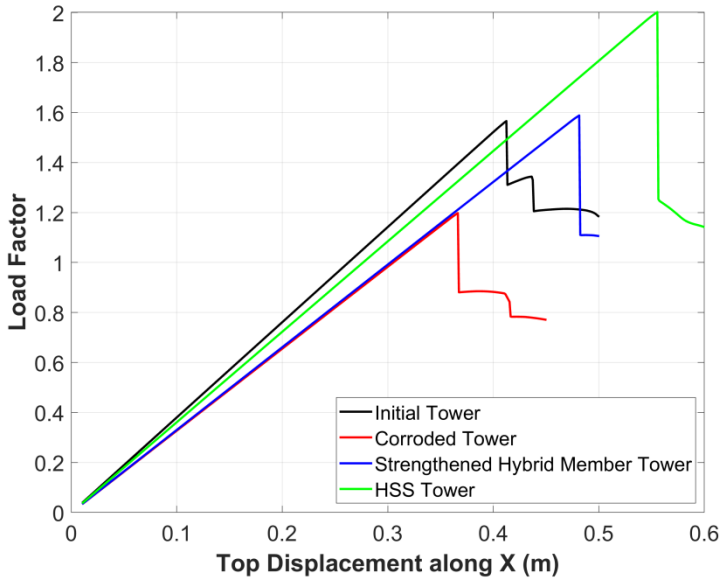

Figure 10: Pushover curves for each of the four towers

For the actual assessment, nonlinear dynamic analyses are employed, assuming a damping equal to 1% based on the results from relevant experiments [40] and experts' recommendation. It is noteworthy that damping is a complex parameter subjected to variations involving the structure's properties and the wind speed. Nevertheless, a single uniform value for damping was considered herein. This was a deliberate measure to reduce the computational effort, since current literature does not report damping to

be one of the top contributing factors to system variability at least compared to local site and weather conditions [41].

The main input for the dynamic analyses is the two horizontal wind speed timeseries (X and Y) created by TurbSim, an example of which along one of the principal axes appears in Figure 11a. The vertical wind speed component was neglected, being of very low magnitude. An IEC Kaimal spectral model was employed, assuming Class B moderate turbulence and a Normal Turbulence Model according to [31]-[32]. Based on this model, TurbSim adjusts the turbulence intensity according to the wind speed value, essentially decreasing it as the 10-min average wind speed increases. The length of each timeseries was 10 minutes (600 seconds). The corresponding timeseries of wind force along the height of the tower were estimated by applying Eqs. (4)-(8) along the two horizontal directions (X and Y). Figure 11(b) presents a typical form of the wind force timeseries at the top horizontal diaphragm of the tower (h=48m). It is noteworthy, that the wind force was ramped up gradually during the first 30sec of the analysis in order to avoid any transient artefacts arising from the sudden application of a high wind load.

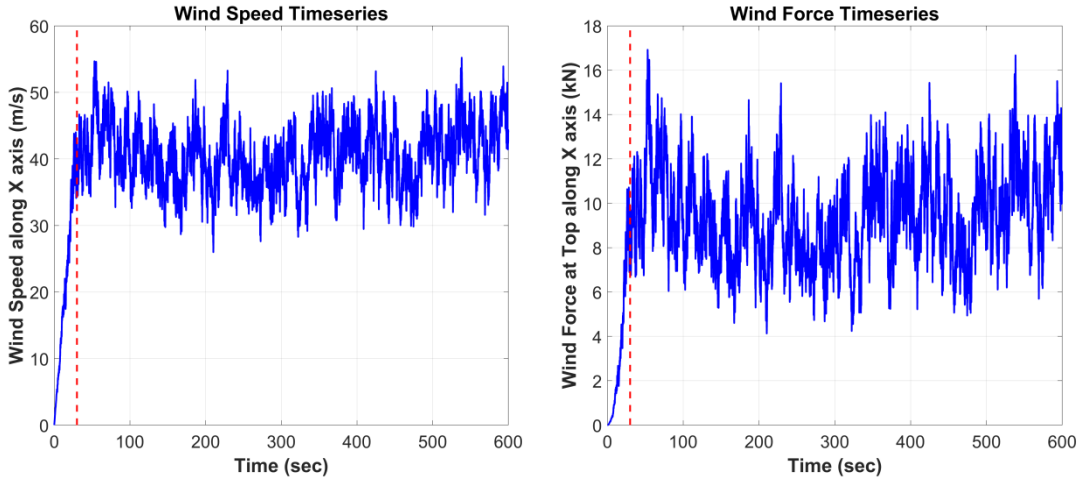

a) b)

Figure 11: Typical a) wind speed and b) wind force timeseries at the height of top horizontal diaphragm of the tower (h=48m). The added ramp-up appears before the 30sec mark indicated by the red dashed line.

In the dynamic analyses the maximum interlevel drift was employed as EDP. The maximum interlevel drift was defined as the maximum along the height of the peak values of drift observed between consecutive horizontal bracing levels. Furthermore, in order to specify if the tower failed during the analysis, two minutes (120 sec) of zero load were added at the end of each wind-force timeseries, allowing a simple free oscillation of the tower. If at the end of the free oscillation the residual drift was close to zero (e.g. of the order of 10^{-5}) then it was assumed that the tower did not fail. The occurrence of member buckling was detected by the appearance of residual drift at the end of the response history analysis and subsequent confirmation of members exceeding their strength. This provides a quick (due to fast post-processing of the results) preliminary check sufficient to determine if the tower enters the plastic stage which is shown by pushover analysis to be practically equivalent to collapse (Figure 10). Figure 12 shows two examples of global response in terms of interlevel drift between two consecutive horizontal bracing levels, showing a non-collapsing case (Figure 12a), evidenced by the near-zero residual drift, versus a near-collapse case

(Figure 12b) where the tower is left at a slant. Normally, one could use the maximum interlevel drift itself, but due to the nature of the model, where we have allowed some post-buckling ductility for reasons of numerical stability, it is often the case that a full collapse of the model is not observed; instead, a (practically unrealistic) large permanent deformation appears. Optimally, both max interlevel drift and the maximum residual should be employed to help define global collapse.

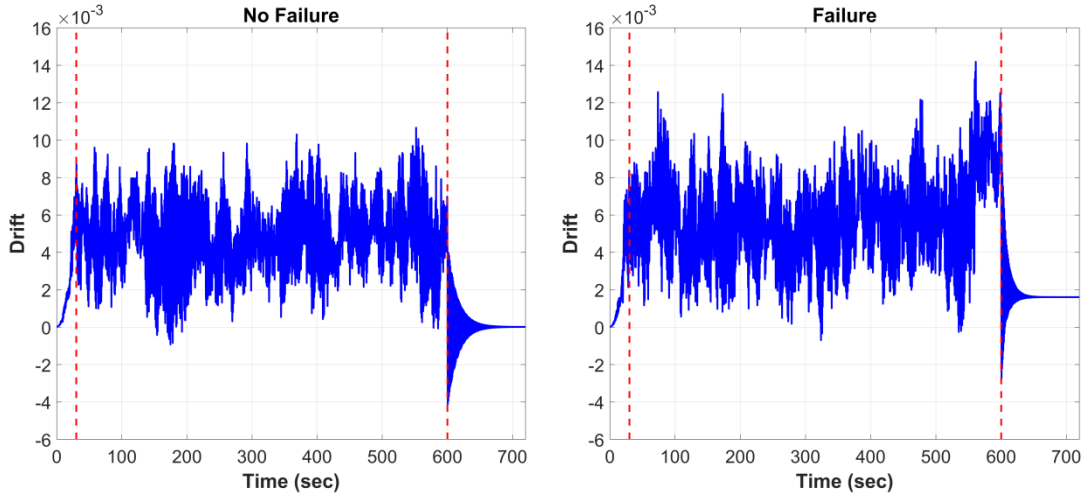

a) b)

Figure 12: Typical drift outputs of the dynamic analysis a) No failure case and b) failure case. The ramp-up part appears before the left red dashed line (30sec), while the free oscillation part comes after the right red dashed line (600sec).

4. SITES AND HAZARD

In temperate/warm climate areas, such as Greece, where ice accretion is not an issue, steel lattice structures are vulnerable to extreme wind conditions. Thus, their risk is primarily dependent on the wind hazard at the site of installation. According to the Greek National Annex [42] of EN1991-1-4 [30] Greece is divided into two wind zones, differentiated by the values of "basic wind speed", V_b, corresponding to the 50-year value of the 10-min average. V_b = 33 m/s for structures located less than 10 km from the shore, and 27 m/s elsewhere.

Sixteen potential sites of installation were selected throughout Greece (Figure 13). At each site, the tower was assumed to be placed with one of its identical faces pointing to the North. Fourteen sites are located on islands or close to the shore (V_b = 33 m/s) and two lie on the mainland mountainous regions (V_b = 27 m/s). All four towers were actually designed for the high-wind coastal zone, thus it is expected that they will not be as challenged by the two inland sites. However, reasons of production standardization, as well as a propensity for damage due to site-specific topographic amplification may often require such measures. Thus, for the sake of comparison, all sites will be included in the assessment.

In order to estimate the probability of occurrence of extreme wind speed values, detailed meteorological data from weather stations installed on the selected sites were employed. The weather stations are administered by the National Observatory of

Athens – NOA [43]. Annual maxima of 10-min wind speed at a height of 10 m, u, were assumed to follow a Gumbel distribution with a probability density function of:

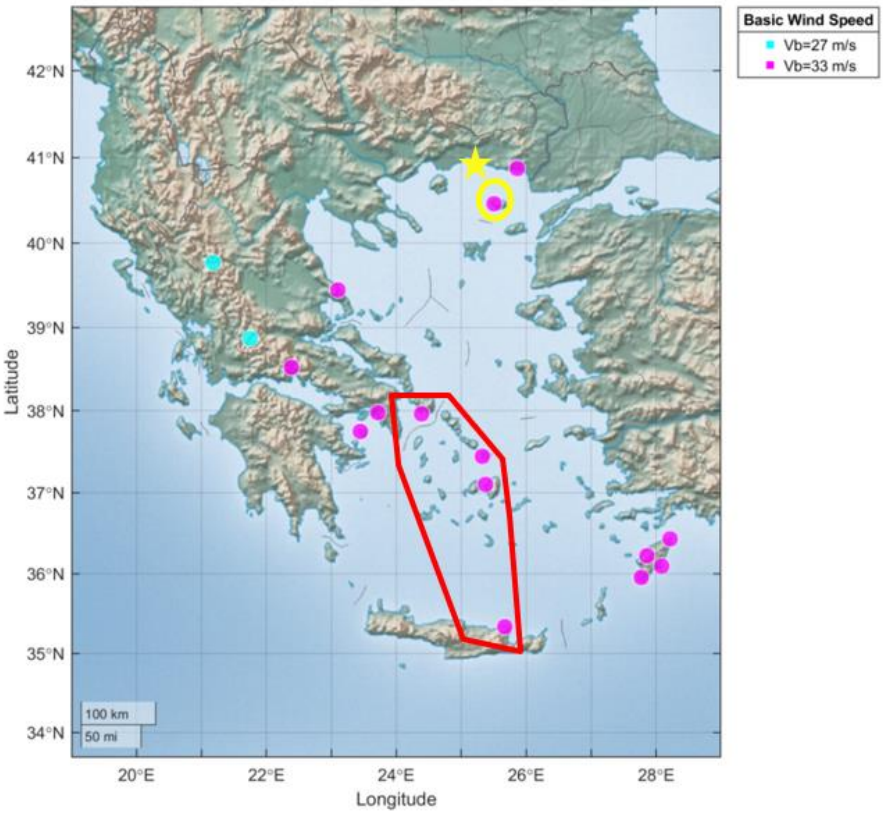

Figure 13: Map of selected sites for potential telecommunication tower installation. The four windiest sites are enclosed by the red polygon. The yellow circle encloses the island of Samothraki and the yellow star denotes the municipality of Komotini (case studies of Section 7).

$$f(u) = \frac{1}{k}\exp\left(-\frac{u-\mu}{k}\right)\exp\left[-\exp\left(-\frac{u-\mu}{k}\right)\right] \tag{9}$$

where μ is the location parameter (indicative of the central value), k is the scale parameter (indicative of the dispersion), and $f(\cdot)$ stands for the probability density function of its argument. It is noteworthy that NOA's network is relatively new and continuously expanding. Thus, detailed wind data was not available for long periods, while the length of the meteorological timeseries was not the same for all stations considered herein. In fact, it varies from 6 and 12 years based on the stations' start date of operation.

Table 3 lists the sixteen sites considered, along with their corresponding μ and k parameters, as estimated by maximum likelihood fitting of the data recorded at each weather station. The values of the Gumbel parameters, and especially μ provide insight on the wind conditions for each site. According to Table 3, the windiest sites of Paximada, Finokalia, Naxos, Mykonos are located mainly in the Central and South-Central part of Greece, on islands or coastal sites (see also Figure 13). It is noteworthy that there is a significant variation in the values of μ, even for sites belonging on the

same wind zone per current code [30],[42]. Finally, it should be noted that the probability of observing meteorological conditions conducive to icing was negligible for all coastal sites and marginal for mountainous ones. Even then, high wind days practically never coincided with potential ice accretion days. Thus, any effects of ice formation were ignored.

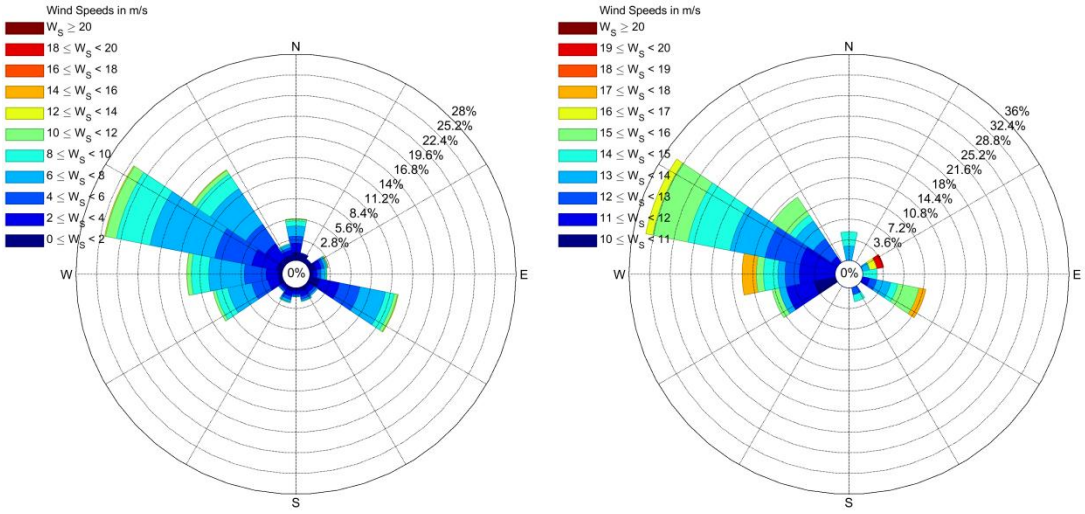

a) b)

Figure 14: Wind roses for a) all 10-min average wind speed values and b) their monthly maxima for the site of Kattavia, island of Rhodes.

Table 3: Characteristics of potential sites of installation

Site	**Latitude (deg)**	**Longitude (deg)**	**Elevation (m)**	**Location Parameter *μ* (m/s)**	**Scale Parameter *k***
Aegina	37.75	23.44	7	14.05	1.54
Alexandroupolis	40.88	25.86	69	11.56	3.37
Amfissa	38.52	22.39	168	9.64	0.64
Athens	37.98	23.72	50	10.70	0.45
Embonas	36.22	27.86	430	21.69	1.39
Finokalia	35.34	25.67	250	34.05	5.40
Karpenisi	38.87	21.75	700	7.68	0.75
Kattavia	35.95	27.77	55	16.93	0.92
Lindos	36.09	28.09	65	18.37	1.52
Metsovo	39.77	21.18	1240	10.57	1.42
Mykonos	37.45	25.33	10	23.69	1.41
Naxos	37.10	25.37	19	25.80	1.94
Paximada	37.96	24.39	220	31.82	3.57
Rhodes	36.43	28.22	95	12.84	0.95
Samothraki	40.46	25.50	90	18.93	2.52
Zagora	39.45	23.10	505	10.46	1.58

It is noteworthy that the values of wind speed u correspond to (annual) maximum values of wind speed. Regarding the combination of maximum wind speed u and direction θ, due to the short length of meteorological timeseries, there is not enough annual data to reliably determine the joint distribution $f(u,\theta)$. Still, a statistical analysis (i.e. wind rose) of monthly maxima against all recorded 10-min average values gave similar distribution of directions θ (Figure 14). Therefore, it was assumed that the distribution of wind directions remains the same for annual maxima as well. Furthermore, due to lack of sufficient data the simplified assumption of the independence between the wind speed and direction was made, rather than adopting a more elaborated correlation model as in [44]. Thus, the joint distribution was considered as $f(u,\theta) = f(u) \cdot f(\theta)$, where $f(\theta)$ corresponds to the empirical distribution (wind rose) of θ per wind station measurements.

5. FRAGILITY ASSESSMENT RESULTS

Given our two IMs of wind speed, u, and wind direction, θ, a two-parameter wind fragility was estimated for each tower via a multi-stripe approach [45]. Discrete levels of u were selected within 20 – 50m/s at steps of 2.5m/s, while three different wind angles of attack, namely: 0°, 22.5° and 45° were deemed to be sufficient for capturing practically all wind angle effects due to the double in-plan symmetry of the towers. At each combination (or "stripe") of u and θ considered, twelve wind-speed timeseries were found to be more than sufficient for the analysis due to the low record-to-record variability. These were simulated with TurbSim, applied at the correct horizontal angle to the tower, and the corresponding dynamic analyses were performed in OpenSees. Then, the probability of failure at the given vector *IM* value of (u, θ), or $P(D > C|u,\theta)$, can be estimated as the fraction of analyses causing failure over the total of 12 [21].

One may directly employ the empirical fragility thus produced, especially if a dense set of *IM* levels was used. Alternatively, one can use larger *IM* steps and fit a lognormal cumulative distribution function [46] to derive a functional form for $P(D > C|u,\theta)$:

$$P(D > C|u,\theta) = \Phi\left(\frac{\ln[u/u_{50}(\theta)]}{\beta(\theta)}\right) \tag{10}$$

where $\Phi(\cdot)$ is the standard normal cumulative distribution function, $u_{50}(\theta)$ is the median of the fragility function which corresponds to the value of *IM* with 50% probability of failure and $\beta(\theta)$ is the logarithmic standard deviation, referred to as *dispersion* of the *IM* failure capacity. The dispersion estimated from fitting the lognormal distribution (Eq. (10)) to the fragility of each wind direction, termed $\beta_R(\theta)$, can be augmented to account for additional sources of uncertainty by taking a first-order assumption [47]. Then, additional uncertainty does not change the central value (median) of the capacity distribution, only increasing its dispersion in a square-root-sum-of-squares fashion:

$$\beta(\theta) = \sqrt{\beta_R(\theta)^2 + {\beta_b}^2 + {\beta_{Cd}}^2 + {\beta_C}^2} \tag{11}$$

Herein, the values of $\beta_R(\theta)$ range between 1% and 4% as revealed by the fragility analyses. The term β_b stands for the dispersion reported in laboratory testing for steel angle buckling resistance [48] and was taken equal to 0.10. The β_{Cd} is the term accounting for the dispersion in the aerodynamic coefficient. A value of 0.12 was considered as suggested by [49] based on experiments assuming normality, but at such low coefficients of variation, normal and lognormal distributions are very close. The

final term β_C, takes into account construction quality, other ancillaries etc. It was taken to be 0.10 equal to the central value advocated by FEMA-P-58-1 [50] for similar cases.

Table 4: Fragility parameters for each of the four tower versions

Wind Angle θ	Initial		Corroded		Strengthened		HSS	
	$u_{50}(\theta)$ (m/s)	$\beta(\theta)$	$u_{50}(\theta)$ (m/s)	$\beta(\theta)$	$u_{50}(\theta)$ (m/s)	$\beta(\theta)$	$u_{50}(\theta)$ (m/s)	$\beta(\theta)$
0°	39.11	0.1895	34.76	0.1921	39.94	0.1856	42.42	0.1857
22.5°	42.83	0.1898	37.41	0.1856	42.41	0.1855	45.43	0.1878
45°	45.94	0.1908	40.08	0.2002	42.94	0.1894	49.89	0.1855

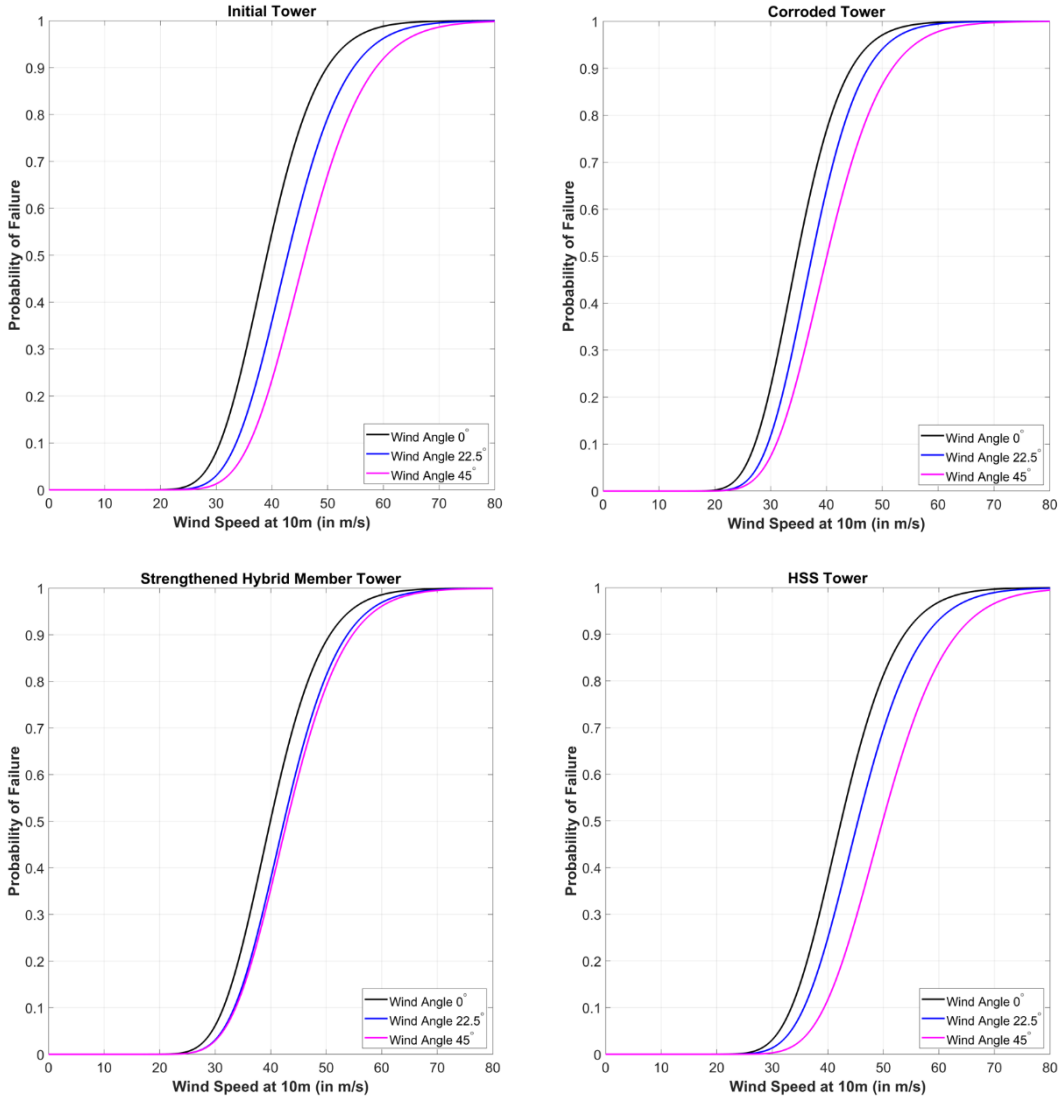

Figure 15: Fragility curves of the four tower case studies

Table 4 summarizes the fragility parameters for each of the four towers considered herein. It is obvious that regardless of the version of tower, the median wind speed of failure is the lowest for a wind angle of 0° (wind perpendicular to the face of the tower). As expected, the values of the median capacity are consistent with the strength of each tower as presented in the pushover curves (Figure 10). Thus, the corroded tower has the

lowest median capacity. Then the initial tower and the strengthened hybrid member tower follow showing almost the same values, while the largest median wind speeds are observed for the HSS tower. This is not necessarily an effect of the higher strength of steel, but rather an arbitrary consequence of taking a different path in design optimization for ease-of-manufacturing. Based on the aforementioned values, the fragility curves of Figure 15 are derived.

6. RISK ESTIMATION RESULTS

Since wind is the only hazard considered, the risk for an immutable non-aging tower under stationary climate conditions is fully quantifiable via Eq. (3). In other words, this application is valid disregarding any potential climate change effects and assuming appropriate corrosion inhibition/stabilization measures have been undertaken so that the four tower types retain their time-of-assessment properties throughout their entire service lifetime of 60 years. Otherwise, one needs to employ a framework that explicitly accounts for fragility evolution due to aging and corrosion (e.g., as per [51] or [52]), as well as for evolving hazard.

In the case at hand, both wind speed (u) and wind angle (θ) were considered as *IM*s, thus Eq. (3) is expressed as follows:

$$\lambda\,(D > C) = \int_{u} \int_{\theta} P(D > C|u,\theta) \cdot f(u,\theta) \cdot du \cdot d\theta \tag{12}$$

If now all the potential values of u and θ are discretized into N and M bins respectively, then Eq. (12) can be written as follows:

$$\lambda\,(D > C) = \sum_{i=1}^{N} \sum_{j=1}^{M} P\big(D > C|u_i,\theta_j\big) \cdot P\big(u_i,\theta_j\big) \tag{13}$$

where: $P\big(u_i,\theta_j\big)$ is the probability of wind to have wind speed u_i and direction θ_j. Considering the aforementioned independence assumption of wind speed and direction, Eq. (13) becomes:

$$\lambda\,(D > C) = \sum_{j=1}^{M} \sum_{i=1}^{N} P\big(D > C|u_i,\theta_j\big) \cdot P(u_i) \cdot P\big(\theta_j\big) \tag{14}$$

Small values of λ are numerically equivalent to the annual probability of failure. Following the typical Poisson assumption for the occurrence of extreme wind events, the reciprocal value of λ corresponds to the Return Period (*RP*) in years:

$$RP = \frac{1}{\lambda} \tag{15}$$

Then, the failure probability during the service life T (in years) of a structure is estimated as:

$$P_{fail} = 1 - e^{-\lambda T} \tag{16}$$

Table 5: Risk estimation results for the initial and the corroded towers. The most critical sites in annual probability of failure are indicated in bold.

Site	Initial Tower			Corroded Tower		
	Annual Probability of Failure	Mean Return Period (yrs)	Failure Probability during Service Life	Annual Probability of Failure	Mean Return Period (yrs)	Failure Probability during Service Life
Aegina	1.82E-05	5.49E+04	1.09E-03	1.18E-04	8.46E+03	7.07E-03
Alexandroupolis	5.86E-04	1.71E+03	3.46E-02	1.84E-03	5.44E+02	1.04E-01
Amfissa	8.21E-11	1.22E+10	4.93E-09	2.21E-09	4.52E+08	1.33E-07
Athens	6.09E-11	1.64E+10	3.65E-09	2.52E-09	3.96E+08	1.51E-07
Embonas	1.79E-03	5.60E+02	1.02E-01	9.51E-03	1.05E+02	4.35E-01
Finokalia	**2.87E-01**	3.49E+00	1.00E+00	**4.68E-01**	2.14E+00	1.00E+00
Karpenisi	4.82E-11	2.07E+10	2.89E-09	8.62E-10	1.16E+09	5.17E-08
Kattavia	1.48E-05	6.75E+04	8.88E-04	1.55E-04	6.45E+03	9.26E-03
Lindos	1.80E-04	5.57E+03	1.07E-02	1.19E-03	8.39E+02	6.90E-02
Metsovo	7.65E-07	1.31E+06	4.59E-05	5.55E-06	1.80E+05	3.33E-04
Mykonos	5.49E-03	1.82E+02	2.81E-01	2.48E-02	4.03E+01	7.74E-01
Naxos	2.36E-02	4.24E+01	7.57E-01	7.66E-02	1.31E+01	9.90E-01
Paximada	**1.71E-01**	5.84E+00	1.00E+00	**3.38E-01**	2.96E+00	1.00E+00
Rhodes	2.43E-07	4.11E+06	1.46E-05	2.98E-06	3.35E+05	1.79E-04
Samothraki	2.00E-03	5.00E+02	1.13E-01	7.63E-03	1.31E+02	3.67E-01
Zagora	1.97E-06	5.07E+05	1.18E-04	1.24E-05	8.07E+04	7.43E-04

Table 6: Risk estimation results for the strengthened hybrid member and the HSS towers. The most critical sites in annual probability of failure are indicated in bold.

Site	Strengthened Hybrid Member Tower			HSS Tower		
	Annual Probability of Failure	Mean Return Period (yrs)	Failure Probability during Service Life	Annual Probability of Failure	Mean Return Period (yrs)	Failure Probability during Service Life
Aegina	1.54E-05	6.51E+04	9.21E-04	4.97E-06	2.01E+05	2.98E-04
Alexandroupolis	6.47E-04	1.54E+03	3.81E-02	2.90E-04	3.45E+03	1.73E-02
Amfissa	5.81E-11	1.72E+10	3.48E-09	7.42E-12	1.35E+11	4.45E-10
Athens	2.08E-11	4.82E+10	1.25E-09	2.99E-12	3.34E+11	1.79E-10
Embonas	1.48E-03	6.76E+02	8.49E-02	5.09E-04	1.96E+03	3.01E-02
Finokalia	**2.96E-01**	3.38E+00	1.00E+00	**2.04E-01**	4.91E+00	1.00E+00
Karpenisi	2.58E-11	3.88E+10	1.55E-09	5.40E-12	1.85E+11	3.24E-10
Kattavia	1.02E-05	9.77E+04	6.14E-04	2.59E-06	3.86E+05	1.55E-04
Lindos	1.90E-04	5.27E+03	1.13E-02	5.28E-05	1.89E+04	3.16E-03
Metsovo	6.26E-07	1.60E+06	3.76E-05	1.91E-07	5.23E+06	1.15E-05
Mykonos	4.62E-03	2.16E+02	2.42E-01	1.75E-03	5.71E+02	9.97E-02
Naxos	2.05E-02	4.89E+01	7.07E-01	9.53E-03	1.05E+02	4.36E-01
Paximada	**1.71E-01**	5.85E+00	1.00E+00	**1.05E-01**	9.49E+00	9.98E-01
Rhodes	1.68E-07	5.96E+06	1.01E-05	4.01E-08	2.49E+07	2.41E-06
Samothraki	2.03E-03	4.93E+02	1.15E-01	8.63E-04	1.16E+03	5.05E-02
Zagora	1.63E-06	6.15E+05	9.75E-05	5.42E-07	1.85E+06	3.25E-05

The results appear in Table 5 and Table 6 for all cases studied. It is evident that, since wind is the governing failure hazard, the probability of failure for a specific version of tower follows the pattern of the wind speed. In specific, the sites with the larger location

parameters (i.e. more adverse wind conditions) show larger probabilities of failure. Moreover, for any given site the failure risk follows the trends shown by tower capacities. The corroded tower always shows the highest probability of failure (and thus the lowest *RP*) while the lowest probability of failure (highest *RP*) occurs in the case of the HSS tower.

Figure 16 shows the risk, in terms of the failure probability during service life, of each of the four towers as depicted on a map. Each site was categorized in one of three risk classes: Low (probability of failure during service life <1%), Medium (probability of failure during service life 1%-50%) and High (probability of failure during service life >50%).

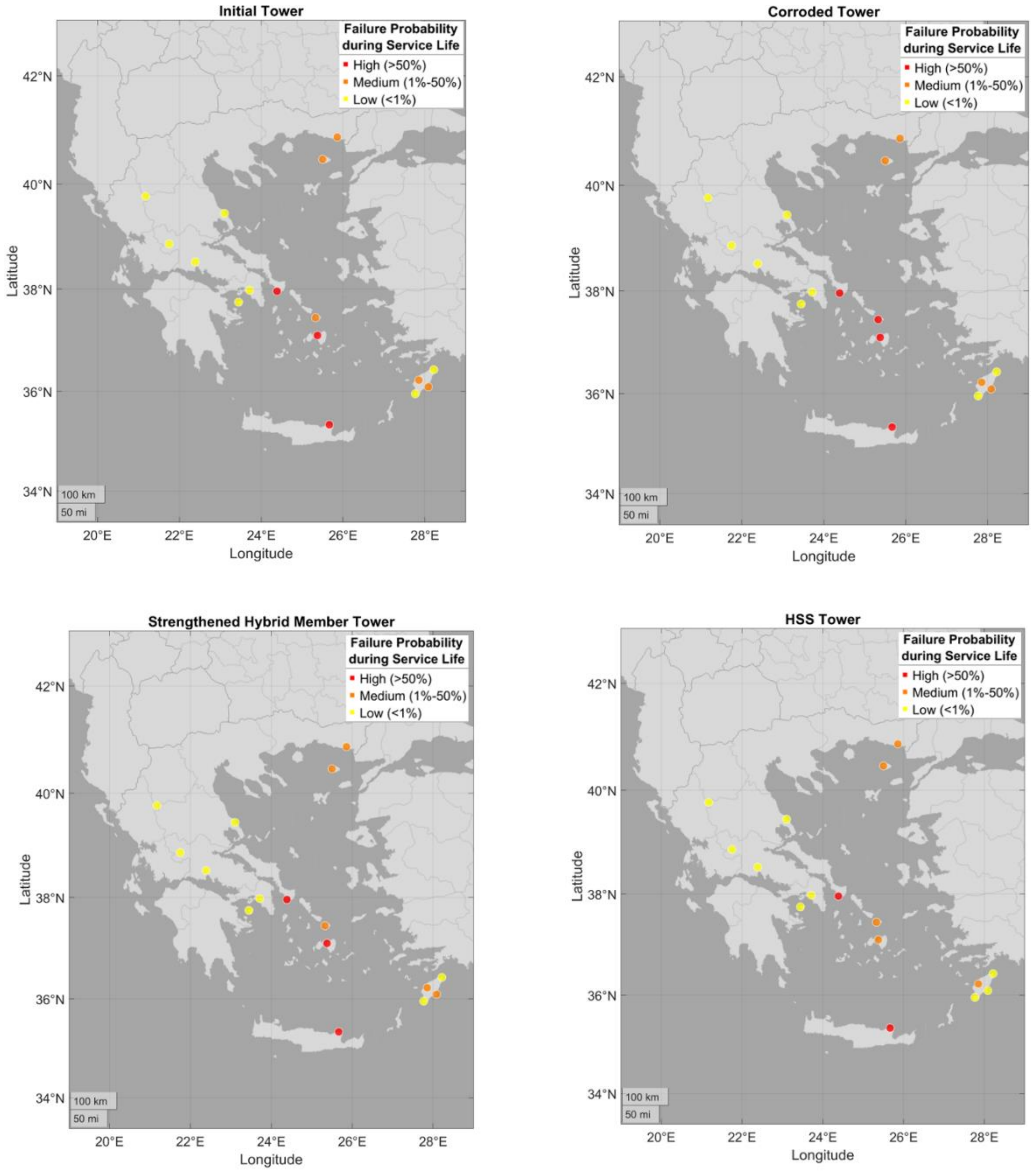

Figure 16: Location of sites indicating failure probability during service life

Based on Figure 16, the initial tower has high risk (red) in three sites: Paximada and Finokalia, where the corresponding failure probability during the service life reaches 100% and in Naxos where the risk is around 76%. On the other hand, five sites (Lindos, Embonas, Mykonos, Samothraki and Alexandroupolis) were categorized in the medium

class (orange) and the rest of sites in the low class (yellow). Regarding the corroded tower, the site of Mykonos moved from the medium to high-risk class, while obviously all failure probabilities increased significantly per Table 5. When the strengthened hybrid member version is considered, the risk classes of the sites are the same as the initial tower, indicating the expected restorative effect of the structural intervention. Finally, regarding the HSS version, two of the sites (Paximada and Finokalia) remain in the high-risk class, while the site of Naxos has transitioned from high to the medium-risk class. In a similar way, the site of Lindos has now moved from the medium-risk class to the low-risk class. In other words, the imperfect structural optimization of the HSS tower has imparted it with higher strength that partially mitigates the discrepancies between the design wind maps and the actual hazard. Still, this is far from ideal and it is not an effect that can be relied upon to mitigate the deficient basis of the Greek National Annex of EN1991-1-4 [41].

7. COST BENEFIT ANALYSIS EXAMPLE

7.1. Baseline rehabilitation options

After exhausting a service life of 60 years, it is assumed that the initially installed telecommunication tower stands corroded. The telecommunication company (owner) needs to take action, facing the next 60 years (or even less) of operation, and is considering the following options:

a. Do Nothing: This is the typical option usually due to lack of funds, or when the risk or consequence of failure is considered to be low despite the corrosion damage.
b. Replace by Conventional: This is a full replacement of the tower with an identical one (initial model), made of the same members and structural steel. The original foundation is kept due to the similar dimensions and little to no corrosion damage.
c. Replace by HSS: This is a full replacement of the tower with a new one made of high-strength steel (HSS) angles. Same as above, the foundation is kept.
d. Strengthen with hybrid members (FRP): This is a partial strengthening scheme, where FRP plates are locally applied to critical corroded members.

Note that a conventional strengthening scheme, whereby critical corroded members would simply be replaced by equivalent non-corroded ones, is not considered. Moreover, other strengthening options that would not involve removal of sections, such as adding angles to critical members to form a stronger battened section, are also not considered.

To price our options, the following basic assumptions are also made:

i. Corrosion progression is inhibited in all cases throughout the lifetime of the towers, employing, e.g. cathodic protection measures for a & d and improved zinc coating for c & d. The cost of such measures is assumed to be the same in all cases and it is thus disregarded for the comparisons that follow, making the cost of the "Do Nothing" approach exactly zero.
ii. Replacing collapsed towers only incurs the cost of the superstructure, as the foundation remains unaffected.
iii. The cost of the FRP is applied in addition to the cost of conventional maintenance/strengthening of the towers, to replace any defective members, and include transportation, labor, preparation of surfaces, protective painting etc.

Currently, the cost of a 50mm x 1.2mm FRP plate is 30 €/m, with an additional 6.3 €/m for the adhesive product.

iv. S460 steel costs around 40 €/ton more than S355 steel at the time of writing. This is roughly 2% more given a market price of 2,000 €/ton of S355 steel. About three quarters of the HSS tower are made of HSS steel, meaning a surcharge of 1.5% over the conventional steel tower on a ton-by-ton basis.

v. Future repair and replacement costs need to be reduced to their net present value for effective comparison. Given the zero (or negative in some cases) interest rates that have been prevalent for the past few years, we have assumed an effective discount rate of ~0.0% for the next 60 years, simplifying the relevant computation. Historically, a more accurate value would be in the order of 3-5% [53].

Direct costs for constructing the conventional telecommunication tower in Greece reflect 2020 market prices and appear in Table 7. To estimate the cost of a new HSS tower, only the procurement/material cost is recalculated in proportion to the lower weight of the HSS design per Table 8, and applying the 1.5% HSS surcharge. For FRP strengthening, the cost of FRP plates and adhesive is summed up with the cost of performing a conventional maintenance/strengthening on an existing tower of the given size, estimated at 20,000€ per 2020 prices.

Table 7: Initial construction costs for new conventional steel versus HSS towers, as well as for strengthening a corroded existing tower, applicable to Greece for 2020.

Task	**Initial direct costs (€)**		
	Conventional	**HSS**	**FRP**
Procurement (manufacturing, bolts etc.)	47,553	44,728	
Transport and Installation	15,076	15,076	20,000
Coloring	6,670	6,670	
Lighting	4,901	4,901	0
FRP application	0	0	5,663
Total (without foundation)	**74,200**	**71,375**	**25,663**
Tower foundation (excavations, grounding etc.)	19,289	19,289	–
Total (with foundation)	**93,489**	**90,664**	**–**

Table 8: Materials needed and initial direct costs for implementing each strategy

Strategy	**Steel weight (kg) or 50mm x 1.2mm FRP plate length (m)**	**Initial direct costs, C_0 (€)**	**Direct losses per event, C_{1D} (€)**	**Indirect losses per event C_{1I} (€)**	
				Samothraki	**Komotini**
Do Nothing	0	0	74,200	35,048	602,271
Replace Conv.	15,140 kg	74,200			
Replace HSS	14,030 kg	71,375			
Strengthen FRP	156 m	25,663			

7.2. Loss assessment

Since, in the case of collapse, a new conventional tower is assumed to be erected, the direct loss per event is always C_{1D} = 74,200 €. On the other hand, indirect losses due to service disruption (i.e. loss of revenue) heavily depend on the size of the population served, and they are likely to supersede the direct losses of tower replacement for any but the most trivial of scenarios. Thus, one small-scale and one large-scale scenario are considered. First is the island of Samothraki (enclosed in the yellow circle in Figure 13), with a population of 2,859 permanent residents, assumed to reach 7,000 over the three summer months resulting in an annual average of 3,894.25 residents. A single tower is assumed to serve the telecommunication needs of the entire island. The second location is the nearby municipality of Komotini (marked with a yellow star in Figure 13), with similar weather characteristics and a population of 66,919 residents. Using informal data and engineering judgement, a representative average revenue per resident of 30 €/month is assumed. Based on discussions with telecommunication experts in Greece, the length of service disruption due to tower collapse is heavily case/failure/location dependent. Herein, a disruption event is assumed to take 9 days, or 0.30 months, to resolve. This may entail, for example, installation of temporary antennas that are eventually replaced by a new conventional tower. During this period, the telecommunication company cannot charge consumers. In other words, each disruptive event costs 30×0.3 = 9 €/resident, assuming there are no additional contractual penalties. Thus, the indirect cost of one disruptive event, C_{1I}, is 3,894.25×9 = 35,048 € for Samothraki, versus the much higher 66,919×9 = 602,271 € for Komotini.

Based on a Poisson occurrence process for storm events and given the 0% interest, one need only divide the single event losses by the corresponding return period to find the Average Annual Loss, *AAL*, assuming each collapsed tower is replaced by a new conventional one, per typical practice:

$$AAL = \frac{C_1}{RP} \tag{17}$$

By aggregating direct (AAL_D) and indirect (AAL_I) losses over a projected service life of T_L = 60 years, and adding the upfront initial costs (C_0), the total aggregated lifetime cost, LC_{60}, per each rehabilitation strategy can be estimated as:

$$\begin{aligned} LC_{60} &= C_0 + (AAL_D + AAL_I) \cdot T_L \\ &= C_0 + (C_{1D} + C_{1I}) \cdot T_L/RP \end{aligned} \tag{18}$$

Table 9: Return period of collapse versus direct/indirect average annual loss, and total lifetime cost per each strategy. Optimal strategies are indicated in bold.

Strategy	Return Period RP (yrs)	Direct AAL_D (€)	Indirect AAL_I (€)		Lifetime Cost, LC_{60} (€)	
			Samothraki	Komotini	Samothraki	Komotini
Do Nothing	131	566	268	4,597	50,033	309,808
Replace Conv.	500	148	70	1,205	87,313	155,396
Replace HSS	1159	64	30	520	77,030	**106,396**
Strengthen FRP	493	151	71	1,222	**38,959**	107,992

Table 9 shows the results for the small-scale (Samothraki) versus the large-scale scenario (Komotini). From a pure monetary standpoint, it all depends on the population served. If there are many residents (Komotini), replacing with a HSS tower is the best option, having the lowest lifetime cost over 60 years closely followed by the selective strengthening with hybrid members. On the other hand, for a smaller service area (Samothraki), strengthening with hybrid members seems to be by far the best option followed by the "Do Nothing" option. Of course, the selection is also affected by the projected lifetime. If a shorter projected lifetime is considered, say T_L = 10 yrs, by applying Eq. (17)–(18), strengthening with hybrid members is now the best option with LC_{10} = 39,384 € for the case of Komotini (followed by the "Do Nothing" option with LC_{10} = 51,635 €, while the HSS option is associated with LC_{10} = 77,211 €). For the small-scale scenario (Samothraki) the "Do Nothing" option comes first with LC_{10} = 8,339 €, followed by selective strengthening with hybrid members option with LC_{10} = 274,879 €.

As expected, when the cost of disruption is sizeable, less comprehensive solutions with a low upfront cost are only viable in the short term. Long-term planning necessitates higher upfront costs to reap future benefits of fewer disruptions. Of course, other non-monetary considerations (e.g., brand reputation, social consequences, community business disruption) or contractual obligations may further shift one's priorities and make the "Do Nothing" approach less desirable even for smaller populations, such as the case of the touristic island of Samothraki.

8. CONCLUSIONS

The risk of steel lattice structures can be estimated by applying a performance-based engineering framework. Herein, four cases of a telecommunication tower having the same topology but different strength were assessed. A number of sites throughout Greek territory with different wind characteristics were examined as potential installation sites.

Risk results revealed that the probability of failure of a specific telecommunication tower is based on both its strength (i.e. fragility) and the characteristics of its location (i.e. wind hazard). For the same type of tower, higher probability of failure is expected in locations characterized by stronger wind. Similarly, for the same location, a telecommunication tower with lower strength is more vulnerable showing larger probability of failure. As expected, any mismatch between design wind maps and actual local measurements can severely hurt the reliability of a design, or even lead to uneconomical ones. Still, even well detailed design maps may fail to account for important local site effects and thus lead the engineer astray. Overall, the framework presented can provide a useful decision tool for telecommunication companies not only in selecting the appropriate type of tower configuration considering the site of installation characteristics but also in optimizing their strategy on rehabilitation interventions on existing towers under a cost-benefit perspective.

ACKNOWLEDGMENTS

This research has been financed by the European Commission through the Programs: a) "ANGELHY - Innovative solutions for design and strengthening of telecommunications and transmission lattice towers using large angles from high strength steel and hybrid techniques of angles with FRP strips" with Grant Agreement

Number: 753993 (Research Program of the Research Fund for Coal and Steel), b) "PANOPTIS - development of a decision support system for increasing the resilience of transportation infrastructure based on combined use of terrestrial and airborne sensors and advanced modelling tools" with Grant Agreement number: 769129 (HORIZON 2020) and c) "HYPERION - development of a decision support system for improved resilience & sustainable reconstruction of historic areas to cope with climate change & extreme events based on novel sensors and modelling tools" with Grant Agreement number: 821054 (HORIZON 2020). The authors gratefully acknowledge COSMOTE Kinites Tilepikoinonies AE for providing expert opinion on construction costs of the telecommunication tower topology of study.

AUTHOR CONTRIBUTIONS

Dimitrios V. Bilionis: Conceptualization, Data curation, Formal analysis, Methodology, Software, Visualization, Writing - original draft. Konstantinos Vlachakis: Data curation, Formal analysis, Methodology, Software, Visualization. Dimitrios Vamvatsikos: Conceptualization, Methodology, Supervision, Validation, Writing - review & editing. Maria-Eleni Dasiou: Methodology, Software, Visualization. Ioannis Vayas: Project administration, Supervision, Writing - review & editing. Konstantinos Lagouvardos: Data curation, Writing - review & editing.

REFERENCES

[1] Szafran, J. An experimental investigation into failure mechanism of a full-scale 40 m high steel telecommunication tower. *Engineering Failure Analysis*, 54, 131-145, 2015. http://dx.doi.org/10.1016/j.engfailanal.2015.04.017.

[2] Szafran, J., & Rykaluk, K. A full-scale experiment of a lattice telecommunication tower under breaking load. *Journal of Constructional Steel Research*, 120, 160-175, 2016. http://dx.doi.org/10.1016/j.jcsr.2016.01.006.

[3] Lorenzo, I. F., Elena, B. C., Rodríguez, P. M., & Parnás, V. B. E. Dynamic analysis of self-supported tower under hurricane wind conditions. *Journal of Wind Engineering and Industrial Aerodynamics*, 197, 104078, 2020. https://doi.org/10.1016/j.jweia.2019.104078.

[4] Tian, L., Zhang, X., & Fu, X. Collapse Simulations of Communication Tower Subjected to Wind Loads Using Dynamic Explicit Method. *Journal of Performance of Constructed Facilities*, 34, 04020024, 2020. https://doi.org/10.1061/(ASCE)CF.1943-5509.0001434

[5] Tsavdaridis, K. D., Nicolaou, A., Mistry, A. D., & Efthymiou, E. Topology optimisation of lattice telecommunication tower and performance-based design considering wind and ice loads. *Structures*, 27, 2379-2399, 2020. https://doi.org/10.1016/j.istruc.2020.08.010.

[6] Dasiou, M.-E., Vayas, I. & Efthymiou, E. Comparative study of wind loading on telecommunication masts according to DIN 4131 and Eurocode 3 [Vergleichende Untersuchungen zur Windbelastung auf freistehende Telekomunikationsmasten nach DIN 4131 und Eurocode 3], *Stahlbau*, 79, 19-24, 2010. https://doi.org/10.1002/stab.200901283

[7] Stamatopoulos, G. N. Assessment of strength and measures to upgrade a telecommunication steel tower. *International journal of steel structures*, 13, 331-340, 2013. https://doi.org/10.1007/s13296-013-2011-8

[8] Klinger, C., Mehianpour, M., Klingbeil, D., Bettge D., Hacker R., & Baer W. Failure analysis on collapsed towers of overhead electrical lines in the region Münsterland (Germany) 2005, *Engineering Failure Analysis*, 18, 1873-1883, 2011. https://doi.org/10.1016/j.engfailanal.2011.07.004

[9] Makkonen, L., Lehtonen, P., & Hirviniemi, M. Determining ice loads for tower structure design, *Engineering Structures*, 74, 229-232, 2014. https://doi.org/10.1016/j.engstruct.2014.05.034

[10] Sundin, E., & Makkonen, L. Ice loads on a lattice tower estimated by weather station data. *Journal of applied meteorology*, 37, 523-529, 1998, https://doi.org/10.1175/1520-0450(1998)037<0523:ILOALT>2.0.CO;2

[11] Cornell, C. A., & Krawinkler, H. Progress and Challenges in Seismic Performance Assessment. PEER Center News, 3(2), 1–4, 2000. http://peer.berkeley.edu/news/2000spring/performance.html

[12] Ciampoli, M., Petrini, F., & Augusti, G. Performance-based wind engineering: towards a general procedure. *Structural Safety*, 33, 367-378, 2011. https://doi.org/10.1016/j.strusafe.2011.07.001

[13] Barbato, M., Petrini, F., Unnikrishnan, V. U., & Ciampoli, M. Performance-based hurricane engineering (PBHE) framework. *Structural Safety*, 45, 24-35, 2013. http://dx.doi.org/10.1016/j.strusafe.2013.07.002

[14] Petrini, F., & Ciampoli, M. Performance-based wind design of tall buildings. *Structure and Infrastructure Engineering*, 8, 954-966, 2012. https://doi.org/10.1080/15732479.2011.574815

[15] Ciampoli, M., & Petrini, F. Performance-based Aeolian risk assessment and reduction for tall buildings. *Probabilistic Engineering Mechanics*, 28, 75-84, 2012. https://doi.org/10.1016/j.probengmech.2011.08.013

[16] Spence, S. M., & Kareem, A. Performance-based design and optimization of uncertain wind-excited dynamic building systems. *Engineering Structures*, 78, 133-144, 2014. http://dx.doi.org/10.1016/j.engstruct.2014.07.026 0141-0296

[17] Ouyang, Z., & Spence, S. M. Performance-based wind-induced structural and envelope damage assessment of engineered buildings through nonlinear dynamic analysis. *Journal of Wind Engineering and Industrial Aerodynamics*, 208, 104452, 2021. https://doi.org/10.1016/j.jweia.2020.104452

[18] Wilkie, D., & Galasso, C. A probabilistic framework for offshore wind turbine loss assessment. *Renewable Energy*, 147, 1772-1783, 2020. https://doi.org/10.1016/j.renene.2019.09.043

[19] Tessari, R. K., Kroetz, H. M., & Beck, A. T. Performance-based design of steel towers subject to wind action. *Engineering Structures*, 143, 549-557, 2017. https://doi.org/10.1016/j.engstruct.2017.03.053

[20] Depina, I., Divić, V., Munjiza, A., & Peroš, B. Performance-based wind engineering assessment of critical telecommunication infrastructure subjected to bora wind. *Engineering Structures*, 236, 112083, 2021. https://doi.org/10.1016/j.engstruct.2021.112083

[21] Bakalis, K., & Vamvatsikos, D. Seismic fragility functions via nonlinear response history analysis. *Journal of Structural Engineering*, 144, 04018181, 2018, https://doi.org/10.1061/(ASCE)ST.1943-541X.0002141

[22] ANGELHY Deliverable 1.3, Report on analysis and design of 6 case studies, *ANGELHY project consortium*, 2019

http://angelhy.ntua.gr/deliverables/WP1/ANGELHY%20-%20D1.3%20-%20Analysis%20and%20Design%20of%206%20case%20studies.pdf

[23] Mazzoni S., McKenna F., Scott M., & Fenves G., Open system for earthquake engineering simulation. User Command-Language Manual, Report NEES grid-TR 2004-21, Berkeley, CA: Pacific Earthquake Engineering Research, University of California, 2006. Retrieved http://opensees.berkeley.edu

[24] Fasoulakis Z., Vamvatsikos D., Papadopoulos V. Stability of single-bolted thin-walled steel angle beam-columns with stochastic imperfections. ASCE Journal of Structural Engineering, 147, 2021, https://doi.org/10.1061/(ASCE)ST.1943-541X.0003061

[25] Bezas M.-Z., Demonceau J.-F., Vayas I., Jaspart J.-P. Classification and cross-section resistance of equal-leg rolled angle profiles. Journal of Constructional Steel Research 185, 2021, https://doi.org/10.1016/j.jcsr.2021.106842

[26] EN 1993-3-1, Design of steel structures - Part 3-1: Towers, masts and chimneys – Towers and masts. European Committee for Standardization (CEN): Brussels, Belgium, 2006.

[27] Holmes J.D., Banks R.W., Roberts G. Drag and aerodynamic interference on microwave dish antennas and their supporting towers, *Journal of Wind Engineering and Industrial Aerodynamics*, 50, 263-270, 1993, https://doi.org/10.1016/0167-6105(93)90081-X

[28] Martin, P., Elena, V.B., Loredo-Souza, A.M., Camano, E.B. Experimental study of the effects of dish antennas on the wind loading of telecommunication towers, *Journal of Wind Engineering and Industrial Aerodynamics*, 149, 40-47, 2016, https://doi.org/10.1016/j.jweia.2015.11.010

[29] Holmes J.D. *Wind loading of structures, Third Edition*, CRC Press, Taylor & Francis Group, 2015. https://doi.org/10.1201/b18029

[30] EN 1991-1-4, Design of steel structures. Part 1-4: General actions – Wind actions. European Committee for Standardization (CEN): Brussels, Belgium, 2005.

[31] Jonkman, B.J. & Kilcher, L. *TurbSim User's Guide: Version 1.06.00*. NREL Technical Report, National Renewable Energy Laboratory, Golden, Colorado, 2012. https://www.nrel.gov/wind/nwtc/assets/pdfs/turbsim.pdf

[32] IEC 61400-1. *Wind Turbines-Part 1: Design Requirements*, International Electrotechnical Commission, Geneva, Switzerland, 2005.

[33] EN 10025. Hot rolled products of structural steels; European Committee for Standardization (CEN): Brussels, Belgium, 2005.

[34] Braconi et al. Optimising the seismic performance of steel and steel-concrete structures by standardising material quality control (OPUS), Research Program of the Research Fund for Coal and Steel, Grant Agreement Number: RFSR-CT-2007-00039, European Commission, Brussels, Belgium, 2013. https://doi.org/10.2777/79330

[35] EN ISO 9223. Corrosion of Metals and Alloys. Corrosivity of Atmospheres. Classification, determination and estimation; European Committee for Standardization (CEN): Brussels, Belgium, 2012.

[36] EN ISO 9224. Corrosion of Metals and Alloys: Corrosivity of Atmospheres: Guiding Values for the Corrosivity Categories; European Committee for Standardization (CEN): Brussels, Belgium, 2012.

[37] ANGELHY Deliverable 2.3, Report on experimental test on hybrid angle beams and columns, *ANGELHY project consortium*, 2020 http://angelhy.ntua.gr/deliverables/WP2/ANGELHY%20-%20D2.3%20-%20Report%20on%20experimental%20tests%20on%20hybrid%20angle%20beams%20and%20columns.pdf

[38] ANGELHY Deliverable 2.4, Proposal for design rules for hybrid angle members, *ANGELHY project consortium*, 2020 http://angelhy.ntua.gr/deliverables/WP2/ANGELHY%20-%20D2.4%20-%20Design%20rules%20for%20hybrid%20angle%20members.pdf

[39] ANGELHY Deliverable 4.4, Design guide and recommendations, *Research ANGELHY project consortium*, 2020, http://angelhy.ntua.gr/deliverables/WP4/ANGELHY%20-%20D4.4%20-%20Design%20Guide.pdf

[40] Taillon J.-Y., Legeron F., Prud'homme S., Variation of damping and stiffness of lattice towers with load level, Journal of Constructional Steel Research, 71, 111-118, 2012. https://doi.org/10.1016/j.jcsr.2011.10.018

[41] Pagnini, L., Repetto, M.P., The role of parameter uncertainties in the damage prediction of the alongwind-induced fatigue, *Journal of Wind Engineering and Industrial Aerodynamics*, 104-106, pp. 227-238, 2012. https://doi.org/10.1016/j.jweia.2012.03.027

[42] Greek National Annex to ELOT EN 1991-1-4:2005 Eurocode 1: Actions on structures - Part 1-4: General actions - Wind actions, 2005.

[43] Lagouvardos K., Kotroni V., Bezes A., Koletsis I., Kopania T., Lykoudis S., Mazarakis N., Papagiannaki K., Vougioukas S., The automatic weather stations network NOANN of the National Observatory of Athens: operation and database. Geoscience Data Journal, 2017. http://doi:10.1002/gdj3.442016

[44] Li, H.-N., Zheng, X.-W., Li, C., Copula-Based Joint Distribution Analysis of Wind Speed and Direction. *Journal of Engineering Mechanics*, 145(5), 04019024, 2019. https://doi.org/10.1061/(ASCE)EM.1943-7889.0001600

[45] Jalayer, F., & Cornell, C.A., Alternative non-linear demand estimation methods for probability-based seismic assessments. *Earthquake Engineering & Structural Dynamics*, *38*(8), pp.951-972, 2009. https://doi.org/10.1002/eqe.876

[46] Baker, J.W., Efficient analytical fragility function fitting using dynamic structural analysis. *Earthquake Spectra*, 31, 579-599, 2015. https://doi.org/10.1193/021113EQS025M.

[47] Cornell, C. A., Jalayer, F., Hamburger, R. O., & Foutch, D. A., Probabilistic basis for 2000 SAC federal emergency management agency steel moment frame guidelines. *Journal of structural engineering*, 128(4), 526-533, 2002. https://doi.org/10.1061/(ASCE)0733-9445(2002)128:4(526)

[48] Paschen, R., Pezard, J., & Zago, P., Probabilistic evaluation on test results of transmission line towers. International Conference on Large High Voltage Electric Systems, 28th Aug. - 3rd Sep. 1988, Paris, France.

[49] Ellingwood, B. R., & Tekie, P. B., Wind load statistics for probability-based structural design. *Journal of structural engineering*, 125(4), 453-463, 1999. https://doi.org/10.1061/(ASCE)0733-9445(1999)125:4(453)

[50] FEMA P-58-1, Seismic performance assessment of buildings Volume 1- Methodology 2nd Ed., *Federal Emergency Management Agency*, 2018

[51] Vamvatsikos D., & Dolsek, M., Equivalent constant rates for performance-based assessment of ageing structures. *Structural Safety*, 33(1): 8-18, 2011. https://doi.org/10.1016/j.strusafe.2010.04.005

[52] Iervolino, I., Giorgio, M., & Chioccarelli, E., Gamma degradation models for earthquake-resistant structures. *Structural Safety*, *45*, pp.48-58, 2013. https://doi.org/10.1016/j.strusafe.2013.09.001

[53] Paté-Cornell, M. Discounting in risk analysis: capital vs. human safety: structural technology and risk. *Waterloo: University of Waterloo Press*, 1984.